REVIEW OF SCIENTIFIC INSTRUMENTS **88**, 053110 (2017)

Filter-based ultralow-frequency Raman measurement down to 2 cm^{-1} for fast Brillouin spectroscopy measurement

Xue-Lu Liu,[1,2] He-Nan Liu,[1,2] Jiang-Bin Wu,[1,2] Han-Xu Wu,[3] Tao Zhang,[3] Wei-Qian Zhao,[3] and Ping-Heng Tan[1,2,a)]

[1]*State Key Laboratory of Superlattices and Microstructures, Institute of Semiconductors, Chinese Academy of Sciences, Beijing 100083, China*

[2]*College of Materials Science and Opto-Electronic Technology, University of Chinese Academy of Sciences, Beijing 101408, China*

[3]*Beijing Key Lab for Precision Optoelectronic Measurement Instrument and Technology, School of Optoelectronics, Beijing Institute of Technology, Beijing 100081, China*

(Received 14 March 2017; accepted 25 April 2017; published online 19 May 2017)

Simultaneous Stokes and anti-Stokes ultralow-frequency (ULF) Raman measurement down to ~2 cm^{-1} or 60 GHz is realized by a single-stage spectrometer in combination with volume-Bragg-grating-based notch filters. This system reveals its excellent performance by probing Brillouin signal of acoustic phonons in silicon, germanium, gallium arsenide, and gallium nitride. The deduced sound velocity and elastic constants are in good accordance with previous results determined by various methods. This system can shorten the integration time of the Brillouin signal with a good signal-to-noise ratio by more than 2000-fold compared to a Fabry-Perot interferometer (FPI). This study shows how a filter-based ULF Raman system can be used to reliably achieve Brillouin spectroscopy for condensed materials with high sensitivity and high signal-to-noise ratio, stimulating fast Brillouin spectrum measurements to probe acoustic phonons in semiconductors. *Published by AIP Publishing.* [http://dx.doi.org/10.1063/1.4983144]

I. INTRODUCTION

Raman spectroscopy has rapidly gained acceptance as a convenient and non-destructive tool to characterize, quantify the chemical composition, and analyze the electron-phonon interaction of material.[1,2] Most Raman research focuses on the vibration modes with a wavenumber above 100 cm^{-1} due to the limitation of the previous technique to approach a lower wavenumber region (<100 cm^{-1}). A Raman mode as high as 7500 cm^{-1} has been detected in graphite whiskers.[3] However, ultralow-frequency (ULF) Raman measurement is still a challenge for most Raman systems, especially for the Raman system of a single-stage spectrometer. Raman spectroscopy in the ULF region has extensive applications in multiple areas of scientific research: pharmaceutical analysis such as polymorph identification[4] and drugs detection,[5] ULF vibration modes in cells and proteins for biological detection,[6] and unique signals from minerals and gems for forensic analysis.[7] Particularly in the material science area, the ULF Raman technique has been widely desired in semiconductor superlattices and nanomaterials. The quality of semiconductor superlattices can be assessed by observing folded acoustic modes[8,9] in a range less than 100 cm^{-1}. ULF shear and layer-breathing modes in two-dimensional materials can also be used to determine the layer number and interlayer coupling in AB-stacked and twisted multilayer graphene[10–12] and transition metal dichalcogenides.[13–19] Up to now, the capability for the Raman measurement down to 5 cm^{-1} has been realized by means of single-stage spectrometer and notch filters based on volume Bragg grating (VBG).[10,13] An ULF Raman system down to 10 cm^{-1} can also be achieved with longpass edge filters.[20] However, due to the technical constraints of optical filters, a lower wavenumber region below 5 cm^{-1}, which is of current interest to the studies of acoustic phonons in semiconductors and two-dimensional materials, is not available for now.

Acoustic phonons usually have a wavenumber in the region of 0–100 cm^{-1}, which can be measured by various methods such as inelastic neutron scattering (INS), electron energy loss spectroscopy, and inelastic X-ray scattering.[21–23] Brillouin scattering is a desirable technique to probe acoustic phonons near Γ point of the Brillouin zone with high energy resolution via inelastic light scattering, enabling the determination of acoustic velocities, elastic moduli, and photoelastic constants in a crystal.[24–26] The wavenumber of acoustic phonons of a semiconductor material excited by a visible laser is usually in the region of 0–5 cm^{-1} or 0–150 GHz based on its momentum conservation law, which is too small to resolve with conventional Raman spectrometers. This limits the application of the filter-based Raman system to detect acoustic phonons by inelastic light scattering.

Brillouin scattering experiments are usually carried out by a scanning Fabry-Perot interferometer (FPI) based on the principle of multiple beam interference, which has an excellent sub-GHz resolution but requires high illumination power and long acquisition time due to the usage of a single channel detector. The throughput efficiency of FPI-based Brillouin instruments is fundamentally limited to less than $1/f$, where f is the finesse of etalon, which in practice cannot be made much greater than about 100 due to limitations

a)Electronic mail: phtan@semi.ac.cn

on the quality of mirror substrates and coatings. The free spectral range (*FSR*) and resolution ($\delta\lambda$) are balanced by the achievable value of finesse f by $f = FSR/\delta\lambda$. Multiple-pass scanning FPIs can enhance the contrast of the instrument by further extinction of the Rayleigh signal, which can reduce the acquisition time to minutes.[27,28] However, its signal-to-noise ratio (SNR) is still limited. The acquisition time always extends to several or tens of hours to get Brillouin signals with high SNR.[29,30] With the reduced dimension and size of two-dimensional materials, micro-Brillouin measurement with high contrast and fast instrumental response is imperative. From the experimental point of view, a filter-based Raman system could take advantage of recent advancements on grating, Raman filters, and a charge coupled device (CCD) with high efficiency to achieve fairly high-level contrast and to cut down the acquisition time, which are traditionally limiting factors in Brillouin spectroscopy. Therefore it would be promising to advance a conventional filter-based Raman system as a practical implementation to probe a micro-Brillouin signal with high SNR and fast acquisition time.

In this paper, we demonstrate the utilization of volume Bragg grating (VBG) techniques in a single-stage spectrometer Raman system with multi-channel CCD for Stokes and anti-Stokes Raman measurement down to 2 cm^{-1} or 60 GHz, which has already approached the Brillouin scattering region. Its capability of ULF measurements is evidenced by probing Brillouin spectroscopy of acoustic phonons in silicon (Si), germanium (Ge), gallium arsenide (GaAs), and gallium nitride (GaN). The corresponding phonon velocity and elastic constants deduced by the acoustic phonon frequency are in good agreement with the previous results obtained by various methods, which indicates that this filter-based Raman system can be served as a fast and nondestructive technique to Brillouin spectrum measurements.

II. INSTRUMENTATION

The traditional approach to performing ULF Raman measurements involves the usage of a triple spectrometer, in which the double subtractive spectrometer is used to reject the laser line as close as 5-10 cm^{-1} from the laser wavelength. However, this greatly reduces the signal intensity compared with the combination of a single-stage spectrometer and a common notch filter, although the latter arrangement usually does not allow one to detect modes below ~150 cm^{-1}. Fig. 1(a) gives the typical transmission spectrum of a common notch filter for 488 nm (Semrock NF03-488E-25) and its spectral bandwidth (wavenumbers between two 50% transmission points) is about ~640 cm^{-1}. Volume Bragg grating (VBG) based BragGrate™ notch filters make it possible for filter-based Raman systems with ULF measurement ability. BragGrate Notch Filter (BNF) is a reflective volume Bragg grating recorded in a bulk of photosensitive silicate glass with a high diffraction efficiency up to 99.99% (OD3–4), which rejects scattered Rayleigh light that may overshadow the ULF signals. As a notch filter, it is designed to suppress only one specific wavelength with an ultra narrow spectral bandwidth and thus offers the advantage of being able to simultaneously access both the

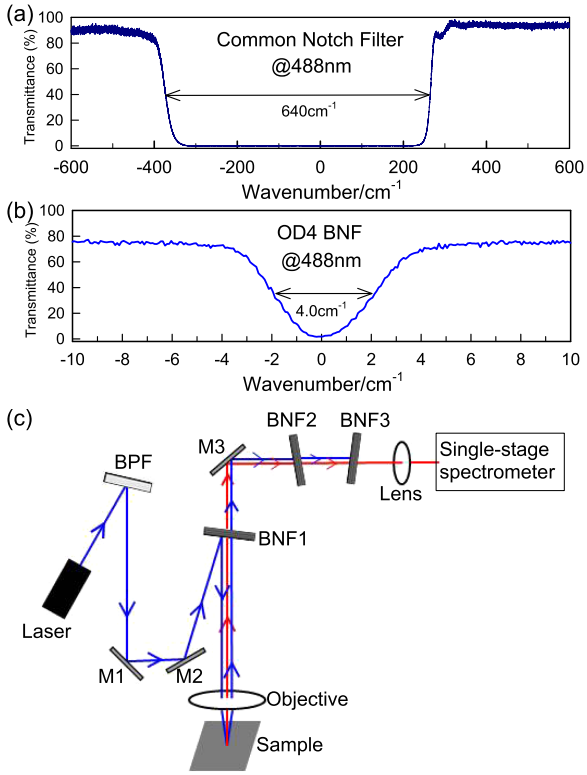

FIG. 1. (a) Transmission spectrum of a common notch filter for 488 nm with a spectral bandwidth of ~640 cm^{-1}. (b) Transmission spectrum of a typical VBG-based BNF for 488 nm with OD > 4 and its spectral bandwidth is about ~4 cm^{-1}. (c) Schematic diagram of optical configuration of the filter-based ULF Raman system. M1, M2, and M3 are the mirrors to align optical paths. BNF1, BNF2, and BNF3 are three VBG-based notch filters. BPF is the VBG-based bandpass filter.

Stokes and anti-Stokes region. Using BNFs in combination with a single-stage spectrometer, the detection of Raman modes down to 5 cm^{-1} was realized in previous research.[10,13] In addition, this BNF is also stable to optical radiation and time degradation, which is superior to the standard notch filters. This setup relies on commercial components and enables us to obtain good signals with low excitation power and short acquisition time. The BNFs used in this work are specially designed to suppress only one specific wavelength and exhibit a spectral bandwidth less than 4 cm^{-1} with an optical density of OD > 4 at 488 nm, a laser line from a Ar^+ laser. To illustrate the low-frequency limit of our system, we measure the BNF's transmission profile with a halogen lamp. The typical transmission spectrum of the BNF @488 nm from OptiGrate Corp is depicted in Fig. 1(b).

The schematic diagram of the experimental setup is shown in Fig. 1(c). First, a BragGrate bandpass filter (BPF) is used to remove plasma lines of the laser, which would appear in the same range of ULF Raman signals and cover the Raman peak of interest with a relatively weaker intensity. The normal bandpass filter has a bandwidth of 200-300 cm^{-1} which is not sufficient. The BPF is also based on volume Bragg grating whose spectral width can be as small as 5-10 cm^{-1}. At least two adjustable mirrors (M1 and M2) are placed before BNF1 to align the laser beam to the center of BNF1.

To provide sufficient elimination of Rayleigh signal, 3 filters with OD3–4 have to be used in sequence. As depicted

in Fig. 1(b), BNF1 exhibits two functions: to reflect the laser beam into the microscope objective and to block the Rayleigh signal from the sample. BNF1 is mounted in a filter holder placed on a horizontal angle variator. The angle variator preliminarily adjusts the incident and reflection angle of BNF1 in order to align the reflected laser beam to the microscope objective. The filter holder has two adjustable screws to further fine-tune the deflection angle to get the best suppression of laser. BNF2 and BNF3 are placed in the signal light path after BNF1 to provide further suppression of the remaining Rayleigh signal and to obtain a high SNR of ULF Raman spectrum. BNF2 and BNF3 are also mounted in angle-adjustable filter holders since the central wavelengths of these BNFs can be altered by several nanometers as their deflection angle changes. When the central wavelengths of the above 3 BNFs are fine-tuned to coincide with the laser wavelength, one can get the best laser attenuation and lowest cut-off wavenumber limit. The ULF Raman signal after BNFs is then focused into the spectrometer for measurement. The spectrometer is equipped with the detector of a charge-coupled device (CCD). The usage of a multi-channel CCD detector prominently shortens the signal acquisition time to subseconds as well as maintains high SNR. Such short measurement time can be expected in the practical applications, as will be described below in comparison with a traditional Brillouin instrument.

A home-modified commercial Jobin-Yvon HR Evolution spectrometer is used as the single-stage spectrometer for ULF Raman measurement. The spectrometer is equipped with a liquid-nitrogen-cooled CCD detector and a 3600 g/mm grating to ensure a spectral resolution of 0.08 cm^{-1} (corresponding to 2.4 GHz) per CCD pixel at 2.54 eV. The excitation wavelength is 488 nm from an Ar^+ laser. The laser power under the objective is less than 1 mW to avoid sample heating. Three BNFs are integrated into the spectrometer as stated above for ULF Raman measurement. A 100× objective lens (Numerical Aperture (NA) = 0.9) is used to focus the laser beam onto the sample and to collect the back-scattered Raman signal for spectral analysis.

III. APPLICATION FOR ACOUSTIC PHONON DETECTIONS

To demonstrate the performance of the BNF-based Raman system for Brillouin spectrum measurement, four very simple semiconductors (silicon (Si), germanium (Ge), gallium arsenide (GaAs), and gallium nitride (GaN)) have been selected for the Stokes and anti-Stokes Brillouin spectra measurements. All the experiments are carried out at room temperature. To determine the mode assignment of the observed Brillouin peaks, we perform polarization measurements for each sample. In our polarization experiment, the scattered light is fixed to be polarized in the laboratory coordinate Y direction with an analyzer. We mainly take two polarization configurations in the backscattering geometry: $Z(YY)\overline{Z}$ (*YY* for short) for the incident laser beam parallel to the laboratory Y axis, $Z(XY)\overline{Z}$ (*XY* for short) for the incident laser beam parallel to the laboratory X axis. Fig. 2 shows the Stokes and anti-Stokes ULF signal in a frequency range of 0–250 GHz of the above four

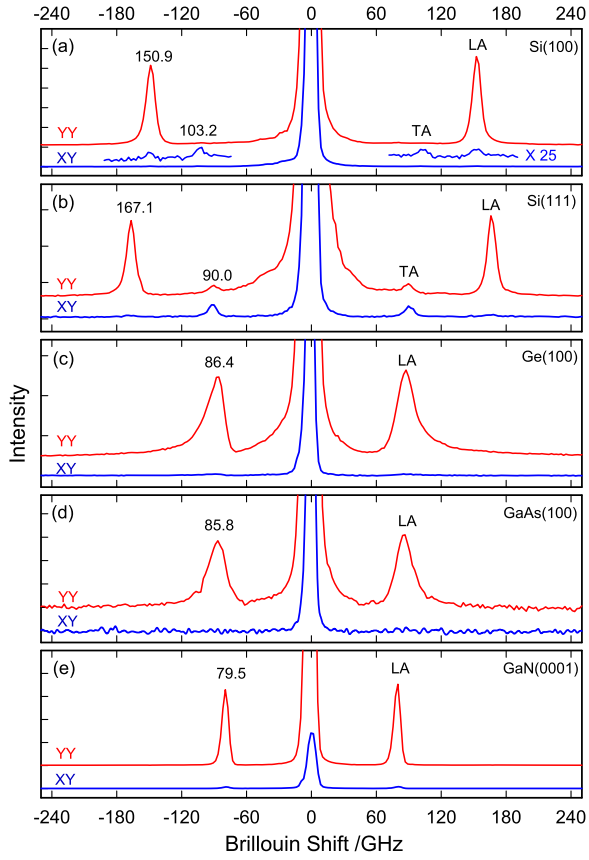

FIG. 2. Polarized Brillouin spectra of Si(100), Si(111), Ge(100), GaAs(100), GaN (0001) in the backscattering geometries of $Z(YY)\overline{Z}$ (YY for short) and $Z(XY)\overline{Z}$ (XY for short).

semiconductors obtained with CCD integration time of several-hundred seconds and a laser power of 1 mW on the sample. Several peaks below 180 GHz are observed. The lowest ULF signal at 79.5 GHz with a fitted full width at half maximum (FWHM) of 6.9 GHz is observed in bulk GaN. The frequency of observed ULF signals in semiconductors is close to that of the corresponding Brillouin peaks, and we assign these peaks as the Brillouin signal from the longitudinal acoustic (LA) or transverse acoustic (TA) phonons in semiconductors. Determination of the Brillouin shifts and FWHM of the Brillouin peak is performed with a Lorentz function. The system resolution of about 2.4 GHz (0.08 cm^{-1}) per CCD pixel is sufficient to resolve a Brillouin peak with FWHM as narrow as down to 6.9 GHz in GaN by curve fitting.

The polarization dependence of Brillouin intensity for the detected acoustic phonons is expressed by[25] $I \propto |\vec{e}_s \cdot B_t \cdot \vec{e}_i|^2/\rho V^2$, where B_t is the Brillouin scattering tensor, and $\vec{e}_s$ and $\vec{e}_i$ are the unit vectors of the polarization direction of scattered and incident light, respectively. ρ is the density, V is the velocity of a certain acoustic phonon mode, $\rho V^2 = \sum_{m,n} c_{mn}$ and c_{mn} is the elastic constants. The Raman scattering tensor[31] is independent of wave vector $\vec{q}$; however, Brillouin scattering tensor B_t depends on the wave vector direction and acoustic phonon propagation direction, which can be derived from a 6 × 6 elasto-optic constant p_{ij} matrix with a given symmetry.[32] For a general wave vector direction, there are three acoustic phonons. One corresponds to the longitudinal sound waves

TABLE I. Brillouin scattering selection rules for backscattering geometry in Z(YY)$\bar{Z}$ and Z(XY)$\bar{Z}$ polarization configuration. $\vec{q}$ is the wave vector direction, $\vec{u}$ is the longitudinal and transverse waves propagation direction. ε_0 and ε_e are the ordinary and extraordinary dielectric constants, p_{ij} is the elasto-optic constant and c_{mn} is elastic constants.

	$\vec{q}$	$\vec{u}$	Z(YY)$\bar{Z}$	Z(XY)$\bar{Z}$
Cubic: Si(O_h) Ge(O_h) GaAs(T_d)	[100]	LA[100]	$\varepsilon_0^4 p_{12}^2/c_{11}$	0
		TA[010]	0	$\varepsilon_0^4 p_{44}^2/c_{44}$
		TA[001]	0	0
	[111]	LA[111]	$\frac{\varepsilon_0^4(p_{11}+2p_{12})^2}{3(c_{11}+2c_{12}+4c_{44})}$	$\frac{4\varepsilon_0^4 p_{44}^2}{3(c_{11}+2c_{12}+4c_{44})}$
		TA$\left[1\bar{1}0\right]$	$\frac{\varepsilon_0^4(p_{11}-p_{12})^2}{2(c_{11}-c_{12}+c_{44})}$	0
		TA$\left[11\bar{2}\right]$	$\frac{\varepsilon_0^4(p_{11}-p_{12})^2}{6(c_{11}-c_{12}+c_{44})}$	$\frac{2\varepsilon_0^4 p_{44}^2}{3(c_{11}-c_{12}+c_{44})}$
Hexagonal: GaN(C_{6v}^4)	[0001]	LA[0001]	$\varepsilon_e^4 p_{33}^2/c_{44}$	0
		TA$\left[2\bar{1}\bar{1}0\right]$	0	0
		TA$\left[\bar{1}2\bar{1}0\right]$	0	0

(LA phonon) and two to the transverse ones (TA phonons). We calculated the selection rules of Brillouin scattering for different wave vector directions and LA/TA phonons using the Brillouin tensor obtained from Ref. 32 and listed them in Table I.

For a cubic crystal, our calculation shows that, in backscattering geometry from its [100] surface, the LA phonon mode should only appear in the *YY* configuration, one of the TA phonons should exist under the *XY* configuration, and the other TA phonon should not appear for either the *YY* or *XY* configuration. In (100)-oriented Si (denoted as Si(100)), only one sharp peak is observed under *YY* at 150.9 GHz with a FWHM of 8.9 GHz. According to the calculation addressed in Table I, in *YY* geometry only the LA phonon is optically allowed, thus we assign it to the LA phonon peak, which corresponds to the longitudinal acoustic mode and travels along the [100] crystallographic axis direction, perpendicular to the sample surface. The amplitude of scattering from TA phonons is zero in *YY* geometry. Under the *XY* configuration, only the TA phonon in the [010] direction can be observed. However, we observed two weak peaks at 103.2 GHz and 150.9 GHz. As the transverse waves travel slower than the longitudinal waves thus having lower Brillouin shift, we assign the 103.2 GHz peak to be TA phonon mode in the [010] direction. The TA phonon in the [001] direction should not be observed here because it is forbidden under both *YY* and *XY* configurations. The higher peak at 150.9 GHz exhibits identical Brillouin shift to the LA phonon in the *YY* configuration and thus the peak is attributed to the LA phonon mode. The appearance of the LA peak in the *XY* configuration can be attributed to the high NA of the objective used, which allows LA phonons to be slightly involved in the *XY* configuration. The same principle can be applied to other semiconductors and we assign their respective LA phonon at 87.3 GHz (FWHM ~ 19.5 GHz) for (100)-oriented Ge (denoted as Ge(100)) and 85.8 GHz (FWHM ~ 17.7 GHz) for (100)-oriented GaAs (denoted as GaAs(100)). Bandwidth increasing and asymmetrical lineshape are known as opacity broadening resulting from their intrinsic larger absorption at 488 nm than Si.[33,34]

As for backscattering geometry from the [111] surface of the cubic crystal, two peaks appear under both *YY* and *XY* configurations. Considering both the frequency values and selection rule, the observed peak at 90.0 GHz is assigned to the TA phonon in $\left[11\bar{2}\right]$ direction and 167.1 GHz to the LA phonon in the [111] direction. Their relative intensities are different due to the different elasto-optic elements p_{ij} and elastic constants c_{mn} associated with each mode. For hexagonal wurtzite (0001)-oriented GaN (denoted as GaN(0001)), in backscattering the *YY* configuration from its [0001] surface(C-plane), only the LA phonon should appear, while in the *XY* configuration, all the acoustic phonon modes should be absent. Therefore, the narrow peak at 79.5 GHz with FWHM of ~6.9 GHz is assigned to its LA phonon. The FWHM of the above Brillouin peaks is comparable to the previous analysis in a FPI system.[29,30]

It must be noted that our system is based on a confocal Raman system in which the microscope with high NA objective is an essential component to increase Raman intensity and spatial resolution. High NA would introduce Brillouin spectral broadening effects because the frequency shift is dependent on the scattering angle.[27] This is an unavoidable case in a confocal system. Indeed, previous research has found that peak displacement and lineshape broadening are minimized in a 180° backscattering geometry compared to a 90° geometry.[35] In this case, peak displacement is estimated to be about 2% and broadening of the FWHM about 0.8 GHz for NA = 0.9 used in our system.[35] As the LA and TA phonons of these studied semiconductors distribute around 100 GHz, the relevant peak shift introduced by NA is quite small and also can be estimated. Thus, we do not consider the influence of NA on the frequency determination and spectral broadening. We also use a pinhole of 40 μm to minimize spectral broadening in FWHM of Brillouin peaks.

An acoustic phonon study can provide information about mechanical properties of the material, including the speed of sound, adiabatic compressibility, and the elastic modulus. The magnitude of the phonon wave vector $\vec{q}$ in a backscattering geometry is $q = \frac{4\pi}{\lambda}\sqrt{\eta^2+\kappa^2}$, where λ is the incident laser wavelength.[33] $n(\lambda) = \eta + i\kappa$ is the complex refractive index of semiconductors, which varies with λ. η and κ values used in our calculation at $\lambda = 488$ nm are listed in Table II from Refs. 36–39. In Brillouin scattering, the wave vector locates at the very close region near the Γ point of the Brillouin

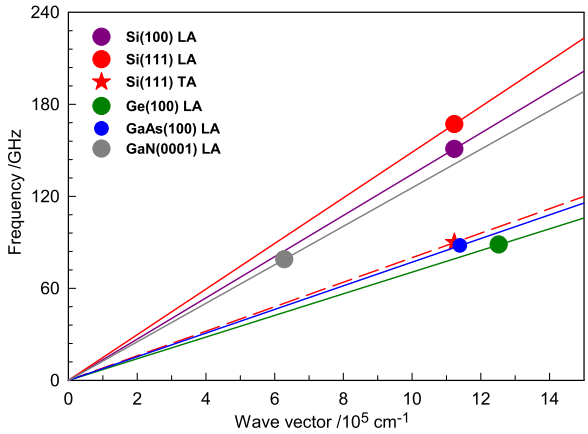

FIG. 3. Phonon dispersion of the LA phonons in Si, Ge, GaAs, and GaN and TA phonons in Si linearly extrapolated from each experimental frequency of the corresponding phonons depicted in Fig. 2 and summarized in Table II.

zone. Within this finite region, the acoustic phonon dispersion maintains a linear dispersion with the wave vector, which is distinct from the optical phonon almost independent of the wave vector. The simulated phonon dispersions of the LA and TA modes of the four semiconductors are depicted in Fig. 3. The slope corresponds to the phase velocity V given by $V = \frac{\Omega_q}{q} = \nu \cdot \Lambda = \frac{\nu\lambda}{2\sqrt{\eta^2+\kappa^2}}$, where ν is the phonon frequency and Λ is the phonon wavelength. Thus the propagation velocity of an acoustic phonon, which is also the speed of sound in the lattice, can be determined by the experimental acoustic phonon frequency. The sound velocities of the present work and those obtained from other methods such as FPI, ultrasonic, and INS methods[40–43] are summarized in Table II for comparison. Our results are consistent with previously-reported values.

Once the mass density ρ of semiconductors is known, the corresponding elastic constants c_{mn} can be evaluated. Acoustic phonons in different directions have particular combination of elastic constants. In cubic Si(100), Ge(100), and GaAs(100), c_{11} corresponds to a LA phonon velocity with $c_{11} = \rho V_{LA}^2$. Their respective elastic constants are evaluated to be $c_{11} = 16.94 \times 10^{11}$ dyn/cm^2 in Si ($\rho = 2.329 \times 10^3$ kg/m^3), $c_{11} = 10.2 \times 10^{11}$ dyn/cm^2 in Ge ($\rho = 5.323 \times 10^3$ kg/m^3), and $c_{11} = 11.9 \times 10^{11}$ dyn/cm^2 in GaAs ($\rho = 5.317 \times 10^3$ kg/m^3). As for Si(111), $(c_{11} - c_{12} + c_{44})/3 = \rho V_{LA}^2$ corresponds to the LA phonon and $(c_{11} + 2c_{12} + 4c_{44})/3 = \rho V_{TA}^2$ to the TA phonon, and thus $c_{12} = 6.78 \times 10^{11}$ dyn/cm^2 and $c_{44} = 7.94 \times 10^{11}$ dyn/cm^2 can be obtained, respectively. In wurtzite GaN(0001), for the LA phonon, $c_{33} = \rho V_{LA}^2 = 38.9 \times 10^{11}$ dyn/cm^2 with $\rho = 6.15 \times 10^3$ kg/m^3. These values are in good agreement with the values in previous works by other techniques.[44–49]

This filter-based ULF Raman system is so sensitive that the weak TA phonon peak can be observed in Si(100) and Si(111), as demonstrated in Fig. 2. To compare the detection sensitivity between the FPI and filter-based Raman systems, we measured the Brillouin signal from the same transparent GaN(0001) and opaque Ge(100) by the filter-based ULF system and a (3+3)-pass tandem FPI (*TFP-1*, JRS Scientific Instruments) integrated with a microscope probe. In this FPI system, the excitation laser is 532 nm (Verdi G SLM, Coherent) with an illumination power of about 8.6 mW at sample. The same type of objective is used in both measurements. As shown in Fig. 4(a), for GaN(0001), the acquired spectrum with a sub-GHz resolution shows the Stokes and anti-Stokes Brillouin peaks at 70 GHz with FWHM ~3.0 GHz, in accordance with the estimated LA phonon frequency at 532 nm excitation. Although each scanning time for the range of about 400 GHz can be accomplished within a second, the depicted spectrum is obtained by intensity accumulation under manifold circles of scanning. The total acquisition time for the present spectrum GaN(0001) is around 800 s (green solid line). In our filter-based ULF system, to perform the comparison, the illumination power of 488 nm excitation is set to about 7.5 mW at a sample under the same type of objective (NA = 0.8). As shown in Fig. 4(b), the Brillouin peak at 79.5 GHz with FWHM of ~8.7 GHz (blue solid line). We acquire Brillouin signals with similar intensity counts with an acquisition time of only 0.3 s, reaching a satisfactory SNR relative to that measured by the JRS FPI system. If we define the SNR as the ratio of peak intensity (μ) of the Raman signal to standard deviation (σ) of the noise where the Raman signal is zero, i.e., SNR = μ/σ. In Fig. 4(a), σ of the spectra measured by FPI and filter-based Raman systems are obtained as 4 and 2, respectively. The deduced SNR of the filter-based Raman measurement is about twice as much as that of the FPI measurement. The acquisition efficiency of the filter-based ULF system drastically increases by more than 2000-fold without any significant losses in the detection quality (accuracy) compared to the JRS FPI system.

TABLE II. Value of the complex refractive index $n(k_i) = \eta + i\kappa$, wave vector q, Brillouin shift ν, acoustic phonon velocity V from present work, and data obtained from previous work by various methods (FPI: Fabry-Perot interferometer, US: Ultrasonic, INS: inelastic neutron scattering).

					V(10^5 cm/s)	
	η	κ	q(10^5 cm^{-1})	ν(GHz)	Present work	Previous work
Si(100)	4.36[36]	0.079[36]	11.23	TA:103.2	5.78	5.84(US)[44]
				LA:150.9	8.44	8.35(FPI),[29] 8.48(US)[41]
Si(111)	4.36[36]	0.079[36]	11.23	TA:90.0	5.04	5.13(INS)
				LA:167.1	9.35	9.40(US)[41]
Ge(100)	4.26[37]	2.35[37]	12.52	LA: 87.3	4.38	4.81 (FPI),[29] 4.97(US)[41]
GaAs(100)	4.40[38]	0.48[38]	11.39	LA: 85.8	4.73	4.68 (FPI),[30] 4.73(US)[42]
GaN(0001)	2.44[39]	0[39]	6.28	LA: 79.5	7.95	7.91(FPI)[50]

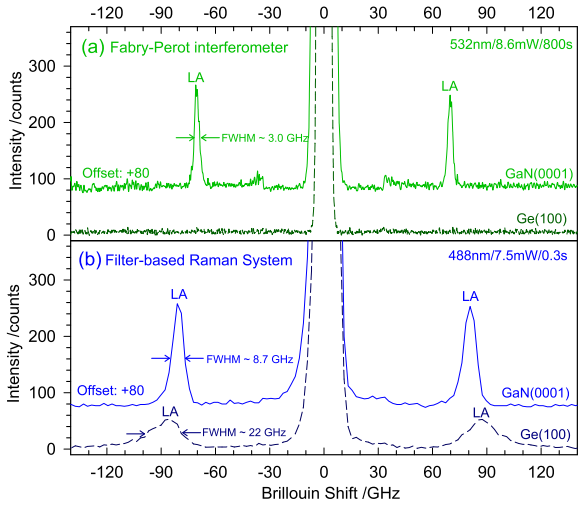

FIG. 4. Brillouin spectra of LA phonons of GaN(0001) and Ge(100) performed by (a) (3+3)-pass tandem FPI (JRS Scientific Instruments) with a 532 nm laser. The acquisition time is 800 s. The laser power is 8.6 mW at sample. (b) The filter-based ULF Raman system with a 488 nm laser. The acquisition time is 0.3 s. The laser power is 7.5 mW at sample.

This also clearly demonstrates that, although the pixel size of the CCD detector is much smaller than that of the single channel detector used in the JRS FPI system, the advantage in multiple channel detection (up to 2000 dependent on the CCD type) and low background at LN_2-cooled detector temperature makes the filter-based ULF system highly efficient to probe acoustic phonons in semiconductors in subseconds.

Although the LA phonon in GaN(0001) can be measured by the JRS FPI system as discussed above, the LA phonon spectrum of Ge(100) is still too weak to be distinguished from the background noise after the acquisition time of 800 s (green dashed line). However, as shown in Fig. 4(b), the LA phonon peak of Ge(100) can be clearly observed by the filter-based ULF system within 0.3 s. Indeed, to obtain the Brillouin signals of opaque materials, such as Si, Ge, and GaAs by a JRS FPI system, a long acquisition time for several or tens of hours was reported.[29] This also demonstrates the high efficiency of the filter-based ULF Raman system to probe the Brillouin signals of opaque semiconductor materials in subseconds.

High laser power used in the Brillouin or Raman system can modify the measured properties of materials. For bulk GaN, it has been observed that the FWHM (8.7 GHz) of the Brillouin peak of its LA phonon excited by 7.5 mW is significantly larger than that (6.9 GHz) excited by 1.0 mW. For ultrathin two-dimensional materials, much lower laser power is necessary to prevent the material being heated or damaged and the laser power less than 0.5 mW is usually used. Therefore, the high acquisition efficiency makes the filter-based ULF system promising in the characterization of ultrathin two-dimensional materials in a micrometer scale.

IV. CONCLUSION

In summary, we have introduced Raman measurement of both the Stokes and anti-Stokes Brillouin components down to ~2 cm^{-1} or 60 GHz with high SNR. The corresponding system is technically based on VBG notch filters, bandpass filters, and a single-stage spectrometer. The system performance is verified by a rapid and reliable measurement of acoustic phonon frequency in four typical semiconductors. The deduced intrinsic properties such as sound velocity and elastic constants are quite consistent with previous reports. The filter-based Raman system reveals its possibilities to serve for fast Brillouin spectroscopy measurements of acoustic phonon and rapid diagnosis of elastic properties for condensed materials, especially for opaque materials.

ACKNOWLEDGMENTS

We acknowledge support from the National Key Research and Development Program of China (Grant No. 2016YFA0301204), National Natural Science Foundation of China (Grant Nos. 11434010, 11474277, 11225421, and 51535002).

[1] A. C. Ferrari and D. M. Basko, Nat. Nanotechnol. **8**, 235 (2013).
[2] X. Zhang, X.-F. Qiao, W. Shi, J.-B. Wu, D.-S. Jiang, and P.-H. Tan, Chem. Soc. Rev. **44**, 2757 (2015).
[3] P. Tan, C. Hu, J. Dong, W. Shen, and B. Zhang, Phys. Rev. B **64**, 214301 (2001).
[4] G. M. Day, J. Zeitler, W. Jones, T. Rades, and P. Taday, J. Phys. Chem. B **110**, 447 (2006).
[5] P. J. Larkin, M. Dabros, B. Sarsfield, E. Chan, J. T. Carriere, and B. C. Smith, Appl. Spectrosc. **68**, 758 (2014).
[6] Y. Shen, P. Upadhya, E. Linfield, and A. G. Davies, Appl. Phys. Lett. **82**, 2350 (2003).
[7] R. L. Frost, Clays Clay Miner. **43**, 191 (1995).
[8] Z. Popovic, J. Spitzer, T. Ruf, M. Cardona, R. Nötzel, and K. Ploog, Phys. Rev. B **48**, 1659 (1993).
[9] P. H. Tan, D. Bougeard, G. Abstreiter, and K. Brunner, Appl. Phys. Lett. **84**, 2632 (2004).
[10] P. H. Tan, W. P. Han, W. J. Zhao, Z. H. Wu, K. Chang, H. Wang, Y. F. Wang, N. Bonini, N. Marzari, N. Pugno, G. Savini, A. Lombardo, and A. C. Ferrari, Nat. Mater. **11**, 294 (2012).
[11] J.-B. Wu, X. Zhang, M. Ijäs, W.-P. Han, X.-F. Qiao, X.-L. Li, D.-S. Jiang, A. C. Ferrari, and P.-H. Tan, Nat. Commun. **5**, 5309 (2014).
[12] J.-B. Wu, Z.-X. Hu, X. Zhang, W.-P. Han, Y. Lu, W. Shi, X.-F. Qiao, M. Ijiaes, S. Milana, W. Ji, A. C. Ferrari, and P.-H. Tan, ACS Nano **9**, 7440 (2015).
[13] X. Zhang, W. Han, J. Wu, S. Milana, Y. Lu, Q. Li, A. Ferrari, and P. Tan, Phys. Rev. B **87**, 115413 (2013).
[14] X. Ling, L. Liang, S. Huang, A. A. Puretzky, D. B. Geohegan, B. G. Sumpter, J. Kong, V. Meunier, and M. S. Dresselhaus, Nano Lett. **15**, 4080 (2015).
[15] C. H. Lui, Z. Ye, C. Ji, K.-C. Chiu, C.-T. Chou, T. I. Andersen, C. Means-Shively, H. Anderson, J.-M. Wu, T. Kidd, Y.-H. Lee, and R. He, Phys. Rev. B **91**, 165403 (2015).
[16] X. Lu, M. I. B. Utama, J. Lin, X. Luo, Y. Zhao, J. Zhang, S. T. Pantelides, W. Zhou, S. Y. Quek, and Q. Xiong, Adv. Mater. **27**, 4502 (2015).
[17] S. Huang, L. Liang, X. Ling, A. A. Puretzky, D. B. Geohegan, B. G. Sumpter, J. Kong, V. Meunier, and M. S. Dresselhaus, Nano Lett. **16**, 1435 (2016).
[18] J.-U. Lee, J. Park, Y.-W. Son, and H. Cheong, Nanoscale **7**, 3229 (2015).
[19] A. A. Puretzky, L. Liang, X. Li, K. Xiao, K. Wang, M. Mahjouri-Samani, L. Basile, J. C. Idrobo, B. G. Sumpter, V. Meunier, and D. B. Geohegan, ACS Nano **9**, 6333 (2015).
[20] M.-L. Lin, F.-R. Ran, X.-F. Qiao, J.-B. Wu, W. Shi, Z.-H. Zhang, X.-Z. Xu, K.-H. Liu, H. Li, and P.-H. Tan, Rev. Sci. Instrum. **87**, 053122 (2016).
[21] J. Axe and G. Shirane, Phys. Rev. B **8**, 1965 (1973).
[22] C. Oshima, T. Aizawa, R. Souda, Y. Ishizawa, and Y. Sumiyoshi, Solid State Commun. **65**, 1601 (1988).
[23] M. Mohr, J. Maultzsch, E. Dobardžić, S. Reich, I. Milošević, M. Damnjanović, A. Bosak, M. Krisch, and C. Thomsen, Phys. Rev. B **76**, 035439 (2007).
[24] R. Vacher and L. Boyer, Phys. Rev. B **6**, 639 (1972).
[25] M. Grimsditch and A. Ramdas, Phys. Rev. B **11**, 3139 (1975).
[26] A. Polian, J. Raman Spectrosc. **34**, 633 (2003).
[27] G. Scarcelli and S. H. Yun, Nat. Photonics **2**, 39 (2008).
[28] Z. Meng and V. V. Yakovlev, Appl. Spectrosc. **70**, 1356 (2016).
[29] M. Kuok, S. Ng, Z. Rang, and D. Lockwood, Phys. Rev. B **62**, 12902 (2000).

[30]M. Kuok, S. Ng, V. Zhang, and D. Lockwood, Solid State Commun. **116**, 27 (2000).
[31]R. Loudon, Adv. Phys. **13**, 423 (1964).
[32]F. T. Arecchi and E. O. Schulz-Dubois, *Laser Handbook* (North-Holland Publishing Company, Amsterdam, 1972).
[33]R. Loudon, J. Phys. Chem. **11**, 403 (1978).
[34]G. Dresselhaus and A. Pine, Solid State Commun. **16**, 1001 (1975).
[35]G. Antonacci, M. R. Foreman, C. Paterson, and P. Török, Appl. Phys. Lett. **103**, 221105 (2013).
[36]D. Aspnes and J. Theeten, J. Electrochem. Soc. **127**, 1359 (1980).
[37]D. Aspnes and A. Studna, Phys. Rev. B **27**, 985 (1983).
[38]J. Theeten, D. Aspnes, and R. P. Chang, J. Appl. Phys. **49**, 6097 (1978).
[39]T. Kawashima, H. Yoshikawa, S. Adachi, S. Fuke, and K. Ohtsuka, J. Appl. Phys. **82**, 3528 (1997).
[40]J. Sandercock, Phys. Rev. Lett. **28**, 237 (1972).
[41]H.-Y. Hao and H. J. Maris, Phys. Rev. Lett. **84**, 5556 (2000).
[42]H. McSkimin, A. Jayaraman, and P. Andreatch, Jr., J. Appl. Phys. **38**, 2362 (1967).
[43]M. Fujii, Y. Kanzawa, S. Hayashi, and K. Yamamoto, Phys. Rev. B **54**, R8373 (1996).
[44]H. McSkimin and P. Andreatch, Jr., J. Appl. Phys. **35**, 2161 (1964).
[45]J. J. Hall, Phys. Rev. **161**, 756 (1967).
[46]K. Jakata and A. Every, Phys. Rev. B **77**, 174301 (2008).
[47]A. Wright, J. Appl. Phys. **82**, 2833 (1997).
[48]K. Adachi, H. Ogi, A. Nagakubo, N. Nakamura, M. Hirao, M. Imade, M. Yoshimura, and Y. Mori, J. Appl. Phys. **119**, 245111 (2016).
[49]M. Yamaguchi, T. Yagi, T. Sota, T. Deguchi, K. Shimada, and S. Nakamura, J. Appl. Phys. **85**, 8502 (1999).
[50]M. Yamaguchi, T. Yagi, T. Azuhata, T. Sota, K. Suzuki, S. Chichibu, and S. Nakamura, J. Phys.: Condens. Matter **9**, 241 (1997).